ORNL/SPR-2022/2446

Report summarizing demonstration of thermal conductivity measurement methods for coated zirconium cladding

Nuclear Technology Research and Development

Prepared for
U.S. Department of Energy
Nuclear Technology R&D Program
Advanced Fuels Campaign

Weicheng Zhong
Hsin Wang
Rebecca McAuliffe
Yong Yan
Stephanie Curlin
Tim Graening
Kory Linton
Andrew Nelson
Oak Ridge National Laboratory

May 2022
M3FT-22OR020202044

ACKNOWLEDGEMENTS

This research was sponsored by the Advanced Fuels Campaign (AFC) Program of the US Department of Energy (DOE), Office of Nuclear Energy. The report was authored by UT-Battelle under Contract No. DE-AC05-00OR22725 with DOE. Takaaki Koyanagi and Xiang Chen performed technical reviews of this report.

SUMMARY

Thermal diffusivity measurements on Zirconium-based cladding materials have historically been a challenge due to the difficulty to measure on specimens with curved geometries, including nuclear grade Zircaloy cladding materials. In this work, we first used Laser Flash Analysis methods to measure the thermal diffusivity of Zircaloy tubes, which show good agreement with Zircaloy plates in this work, as well as previously published data. The consistent results proved the applicability of the Laser Flash Analysis setup for investigating thermal diffusivity of Zircaloy tubes. We further investigate the hydrogen effect on thermal diffusivity of Zircaloy tubes. Hydrogen plays significant roles in temperature dependent thermal diffusivity trends of Zircaloy tube. For low hydrogen concentration, where hydride dissolved into single phase α-Zr at higher temperature, thermal diffusivity is relatively unchanged at low temperature at two phase regions (α-Zr and δ-hydride), and it increases as a function of temperature at single phase α-Zr region. For high hydrogen concentration, where phase transformation (α-Zr + δ-hydride → α-Zr + β-Zr) occurs at 567 ℃, thermal diffusivity decreases as a function of temperature below 567 ℃ before the transformation (α-Zr and δ-hydride), while increase at higher temperature after the transformation (α-Zr and β-Zr).

CONTENTS

FIGURES

REPORT OF THERMAL CONDUCTIVITY MEASUREMENT METHODS FOR COATED ZIRCALOY CLADDING

1. INTRODUCTION

Transfer of heat generated by fission within a nuclear reactor fuel to the coolant governs normal operation and thermal response to possible transients. Operating limits depends on many factors, but foremost is maintaining satisfactory margin to fuel melting. While the coolant temperature is measured at many positions, an accurate understanding of the maximum fuel temperature requires knowledge of both the reactor thermal hydraulics and thermal transport properties of core materials.

Zirconium-based alloys have been used for cladding materials in Light Water Reactors (LWRs) for decades due to their low neutron absorption and good corrosion resistance at the LWRs operational conditions [1]. The thermal conductivity of Zr alloys is conventionally modeled only as a function of temperature [2]; the impact of chemical evolutions or irradiation damage is not considered in fuel performance modeling outside of the impact of waterside oxide coarsening [3]. Recent Accident Tolerant Fuel (ATF) development activities have introduced the concept of coatings to reduce high temperature oxidation of Zr cladding. Proposed coatings span thickness from less than ten micrometers to over fifty [4, 5][cite, cite]. Both ceramic and metallic coatings are under investigation. The effects of coatings on the oxidation resistance has been investigated extensively [6, 7, 8], but the impact of coatings on other properties are only now beginning to receive study. A coating thickness of 50 micrometers would represent approximately ten percent of the nominal cladding thickness. The impact of coatings on thermal conductivity of cladding has been sparely investigated to date despite the importance of thermal transport to reactor safety. Further, the potential for coatings to alter chemical evolution during service or potentially suffer property degradation under irradiation must be fully understood.

The most well understood chemical evolution anticipated of Zr alloys during service is hydriding. During the operation of LWRs, Zircaloy cladding chemically interacts with water coolants and absorbs hydrogen [9]. This behavior has been shown to be reduced if not eliminated by the presence of robust coatings [6]. Due to the limited hydrogen solubility in Zircaloy at the operational temperature, the hydrogen pickup leads to the formation of Zr hydride [10]. Although multiple Zr hydride phases have been reported, including ζ-$ZrH_{0.5}$, γ- ZrH, δ-$ZrH_{1.5-1.7}$, and ε- ZrH_2 [11, 12], δ-phase Zr hydride is of most interest, as it is commonly observed in Zircaloy cladding in nuclear reactors [13]. The dissolution and precipitation of Zr hydride has been studied [14, 15, 16], and their effects on the mechanical behaviors were also investigated [12, 17, 18]. However, the effect of the Zr hydride on thermal conductivity of nuclear grade Zircaloy cladding has not been investigated in the open literature. Unfortunately, the lack of understanding of hydrogen effects is partly because of the difficulty to measure thermal conductivity on a tube geometry of Zircaloy cladding. Previous work demonstrated similar thermal diffusivity between curved and flat specimens for low thermal diffusivity ceramics [19]. But no works has demonstrated the geometry effects for thermal diffusivity of metals that has different thermal transport mechanism.

In contrast to tube geometry Zircaloy cladding, the thermal conductivity has been investigated on plate forms of unalloyed Zr, Zircaloy, and single phase Zr hydride. Unalloyed Zr shows a good thermal conductivity, ~0.2 W/cm/°C, and the alloying elements in Zircaloy-2 and Zircaloy-4 reduce thermal conductivity [20, 21]. The thermal properties of single phase Zr hydride were also investigated up to ~400 °C, which depends on the hydride phase or hydrogen concentration [22, 23, 24, 25]. The single phase δ hydride shows slightly lower thermal conductivity than unalloyed Zr, with little impact from the hydrogen concentrations [22, 23], while the single phase ε hydride shows higher thermal diffusivity than unalloyed

Zr, with higher conductivity for the higher hydrogen concentrations [24, 25]. However, single phase hydride bulk materials have not been reported in commercial reactors. The used Zircaloy cladding in reactors has embedded Zr-hydride phase. Such dual phase Zircaloy cladding has different hydride phase stability and thus different temperature-dependent thermal conductivity properties than single phase Zr hydride.

In this work, we investigated the hydrogen effects on thermal conductivity properties of Zircaloy. Laser flash analysis (LFA) method was used to measure the thermal diffusivity of Zircaloy with different geometries, tube versus plate forms. Zircaloy tubes with different hydrogen concentrations were investigated to examine the hydrogen effects on the thermal diffusivity and electrical resistivity up to 700 ℃. Hydrogen could change the phase stability of Zr and enhance the phase transformation to β-Zr phase at lower temperature in comparison with pure Zr. This phase transformation could change the thermal conductivity properties. However, the hydrogen effects on thermal conductivity have not been investigated. These results will serve as a benchmark to progress to more focused investigation of the impact of coatings. Preliminary results for coated Zr tube are presented for the first time here.

2. MATERIALS and METHODS

2.1 Materials

Zircaloy-4 tubes were procured from Cameco Fuel Manufacturing. The tubes were stress relieved annealed and has a wall thickness of 0.6mm, and outer diameter of 9.5mm. The nominal composition in weight percentage is 1.20-1.45% Sn, 0.07-0.13%Cr, 0.24-0.30%Fe with the balance of Zr, as provided in Ref. [27]. Zircaloy-4 plate was provided by the ATI Corporate. The composition is 1.29-1.39%Sn, 0.10-0.11%Cr, and 0.20-0.23%Fe with the balance of Zr.

Hydrogen charging was performed on Zircaloy-4 tubes at 400-450 ℃, where desired amount of hydrogen was introduced into the samples, with controlling the initial hydrogen gas pressure and temperature profiles. More information of the hydrogen charging process is provided in Ref. [28]. The hydrogen concentration in Zircaloy tubes was measured by the vacuum hot extraction methods followed by the ASTM E1447-05. Zircaloy tubes with three hydrogen concentration were fabricated in this work, they are 331, 1130, and 1820 weight part per million (wppm), designated as 331 wppm H, 1130 wppm H, and 1820 wppm H.

Cr coatings on Zircaloy-4 tubes were included to investigate the Cr coating impact on the thermal diffusivity. Seven-micron Cr coating were deposited on polished Zircaloy-4 tube using the High – power impulse magnetron sputtering (HiPIMS) technique at Acree Technologies Inc. in California as described previously [27].

2.2 Materials characterization.

For thermal diffusivity measurements, tube specimens were cut into 6 mm × 6 mm section in top view using a diamond saw. Figure 1 shows the size of the specimen. For Zircaloy plate, the samples were cut into 12.7 mm discs with a thickness of 2.8 mm. Thermal diffusivity measurements were performed using a Netzsch LFA 467HT apparatus following ASTM E1461. The measurement was performed at 23, 100, 200, 300, 400, 500, 600, and 700 ℃ in argon environment. Temperature was held to the preset temperature for 15 minutes before the measurement. Figure 1 shows the schematic of the flash diffusivity measurement on a tube and a plate geometry respectively. An InSb detector was used to measure the back-surface temperature rise. A detector spot size of 2.7 mm was used to prevent the noise from other components than the sample itself and minimize the effect of sample curvature. Three measurements were performed for each temperature with the deviation below 1%. The Cowan methods was used [29] to fit the detecting signals with the input information including sample thickness and finite pulse width correction for calculating the thermal diffusivity. A representative example of time-dependent signal from flash diffusivity measurement

is shown in Figure 2, along with the fitting results using a Cowan model of pulse width correction. A good fitting is achieved for all samples, with one of the examples shown in Figure 2.

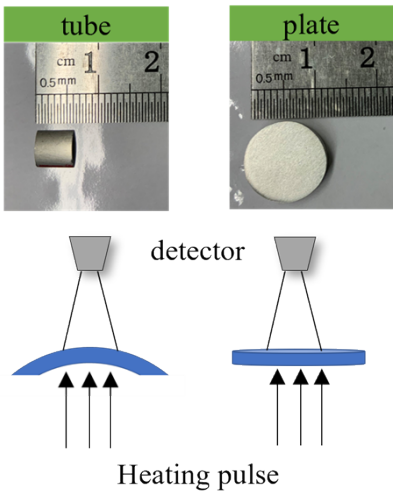

Figure 1. Tube and plate geometries of Zircaloy-4 for the LFA measurement, and the schematics of the LFA setup.

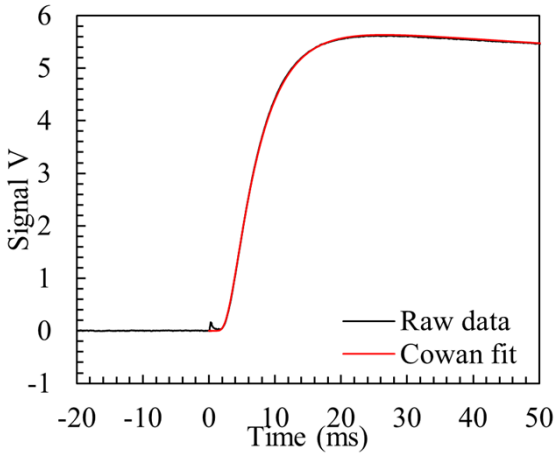

Figure 2. An example of the time dependent LFA raw data and the fitting curve using the Cowan model.

Electrical resistivity was performed in a ULVAC ZEM-3 system on Zircaloy-4 using a four-probe configuration method. The current probes are 4 mm x 4 mm nickel blocks. Two R-type thermocouples were used to measure sample temperature with spacing from 3 mm to 8 mm. One wire of each thermocouple was also used as voltage probe. Measurement temperature is the average of the two thermocouples. No additional temperature coefficient of resistance (TCR) is needed. These measurements were performed in a static helium environment of -0.9 MPa. Tube specimens were cut into 20 mm long and thin strips along the longitudinal directions for the measurement. The differential scanning calorimetry (DSC) was also performed on the hydrogen-charged Zircaloy-4 sample to investigate the phase transformation. The ramping rate was set as 20 °C/min. To characterize the hydride phase, X-ray diffraction were performed on all three hydrogen-charged Zircaloy tubes and reference Zircaloy tube using a Rigaku SmartLab diffractometer with Cu-Kα radiation with a step size of 0.01 degree. Samples for XRD have the same dimension as those for LFA measurement.

3. THERMAL PROPERTIES MEASUREMENTS

3.1 Sample geometry effects

Thermal diffusivity measurements were performed on Zircaloy-4 tube and Zircaloy-4 plates, as the results shown in Figure 3a. Zircaloy-4 tube follows the same trend as the plate, with slightly lower diffusivity for the tube geometry by less than ~5 %. This small difference could be attributed to the different processing methods of different geometry materials or the small composition differences. To calculate the thermal conductivity k, we use the formula $k = \alpha\rho C_p$, where α is the measured thermal diffusivity, ρ is the density, and C_p is the specific heat capacity. Using the reported C_p in Ref. [21] via the interpolation method, the calculated thermal conductivity of Zircaloy-4 tube and plates are shown in Figure 3b, along with previously published data on Zircaloy-4 and unalloyed Zr plates. The results in this work are in a good agreement with the previous measurement on Zircaloy-4 plate [21]. In general, Zircaloy-4 shows a lower thermal conductivity than unalloyed Zr [20, 23, 25], and the difference is smaller at higher temperature. In comparison to Zircaloy-4, the unalloyed Zr exhibits slightly larger deviation between different sources [20, 23, 25]. This might be attributed to the different impurity levels of Zr for different works. Prior works show the effects of impurity levels on thermal conductivity of Ni [30, 31], although the effects on Zr has not been investigated. More importantly, the consistent results of different geometries (tube versus plate) proved the applicability of the flash diffusivity setup for investigating samples of curved geometry and it is suitable for investigating the commercially used Zircaloy tubes after the service in nuclear reactors.

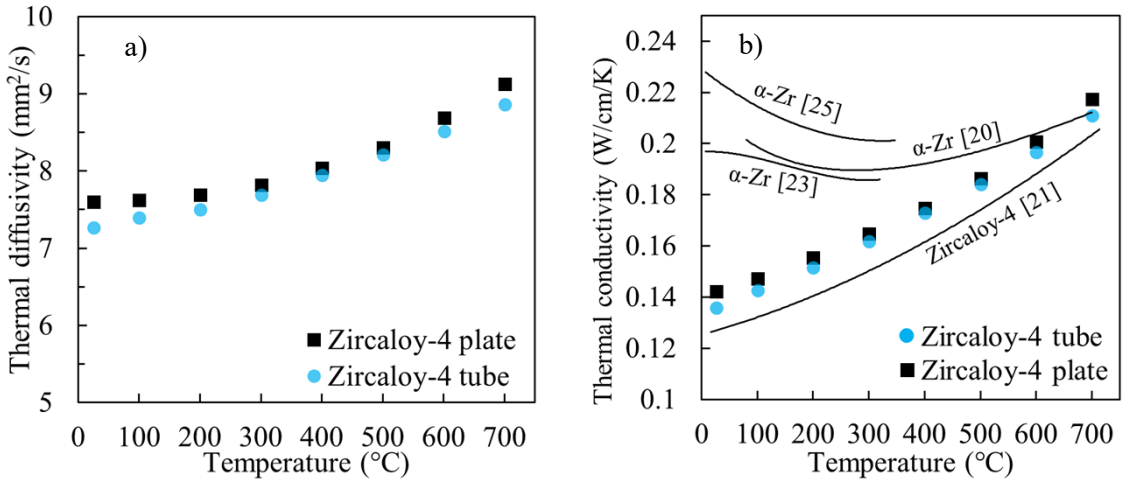

Figure 3. a) Thermal diffusivity of Zircaloy-4 tubes and plates. b) Thermal conductivity of Zircaloy-4 tube and plate in this work, along with previously published data on the Zircaloy-4 plate [21], and unalloyed Zr plates [20, 23, 25].

Electrical resistivity measurements of Zircaloy-4 tube and plate specimens were also performed up to 700 °C. Both geometries show similar temperature-dependent trends of increasing electrical resistivity as a function of temperature. The resistivity values are also in good agreement with previously published data on Zircaloy-4 plate [32].

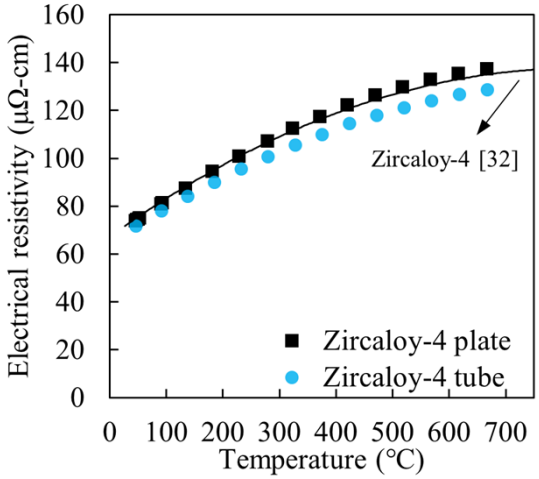

Figure 4. Electrical resistivity of Zircaloy-4 tubes and plates in comparison to the previously published data on Zircaloy-4 plate [32].

Thermal conductivity has two contributions, electron and phonon contributions. To understand their individual contributions in Zircaloy-4, we calculated the electron contribution k_e using the formula $k_e = LT/\rho$ based on the Wiedemann-Franz law, where T is the temperature, ρ is the electrical resistivity, and Lorenz number $L = 2.45 \times 10^{-8}\, W/K^2$ [32]. The phonon contribution k_p is obtained by subtracting the electron contribution from the total conductivity in Figure 3b. The results are shown in Figure 5, with the solid lines for electron contribution, and the dashed lines for phonon contributions. Zircaloy-4 tube and plate in this work have primary conductivity from electron contribution, which agrees with the previous measurement on Zircaloy-4 plates [32]. For the investigated temperature range up to 700°C, the phonon contribution remains almost constant, while the electron contributions increase, which causes an increase of thermal conductivity.

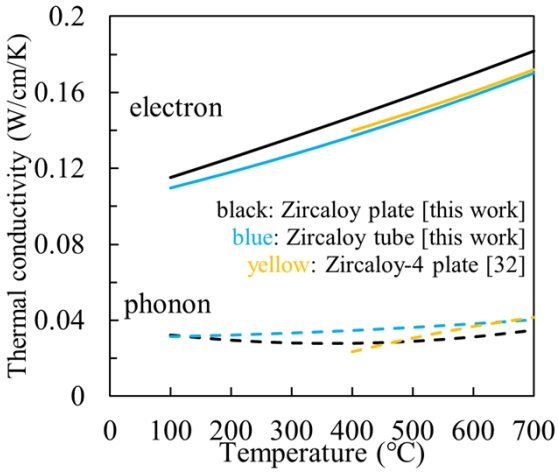

Figure 5. Electron and phonon contributions on Zircaloy tube and plate, in comparison to previously published data on Zircaloy-4 plate [32]

3.2 Hydrogen effects

Hydrogen charging was performed in Zircaloy-4 tubes to three different concentrations: 331 wppm, 1130 wppm, and 1820 wppm. In order to the determine the hydride phase, X-ray diffraction was performed on

these hydrogen-charged Zircaloy-4 tubes in addition to the reference Zircaloy-4 sample. Figure 6 shows that only δ-hydride phase form from the hydrogen charging. Four non-overlapping hydride peaks were identified, as labeled in Figure 6. These peaks are {111}, {200} , {220} and {311} respectively from low to high 2θ angle. No noticeable hydride peak was observed for the 331 wppm H sample, which is likely attributed to the low volume fraction of the hydride phase.

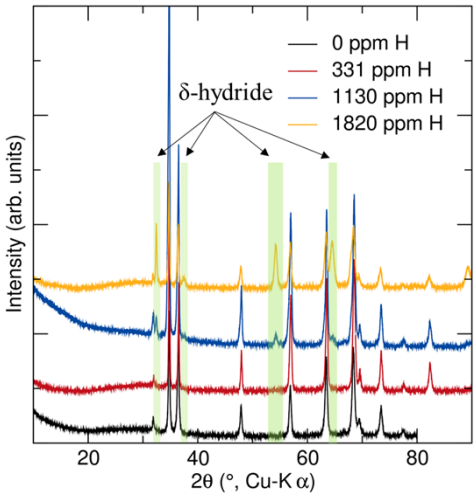

Figure 6. X-ray diffraction of hydrogen-charged and reference Zircaloy-4 samples.

Thermal diffusivity results of hydrogen-charged and reference Zircaloy-4 samples are shown in Figure 7a. The 331wppm H sample shows similar thermal diffusivity as Zircaloy-4 at room temperature, and the thermal diffusivity remains relatively unchanged up to ~400 °C, and it starts to increase at higher temperature. The temperature-dependent trend for 331 wppm H is similar to Zircaloy-4 at 400 °C and above, with lower diffusivity for 331 wppm H. The 1130 wppm H and 1820 wppm H samples exhibit similar temperature-dependent trend, which are distinct to Zircaloy-4 reference and 331 wppm H samples. The diffusivity of both 1130 wppm H and 1820 wppm H decrease to the minimum at ~500 °C and then increase at higher temperature. Electrical resistivity was also measured on the hydrogen-charged Zircaloy-4, as shown in Figure 7b. For Zircaloy-4 and 331 wppm H, the electrical resistivity increases as a function of temperature, whereas for 1130 wppm H and 1820 wppm H, the resistivity increases until at 570 °C, where the resistivity starts to decrease. This turnover temperature is similar to where the thermal diffusivity trend change was observed (see in Figure 7a).

Temperature-dependent thermal diffusivity and electrical resistivity of the hydrogen-charged Zircaloy 4 samples are closely relevant to the hydrogen solvus in Zircaloy-4. The change of the trends at similar temperature for both thermal diffusivity and electrical resistivity measurements motivate us to investigate further on the phase stability. Figure 8a shows the Zr – H binary phase diagram from Ref [12, 33]. Three vertical lines are added in Figure 8a to indicate the hydrogen concentrations at 331wppm H, 1130 wppm H and 1820 wppm H. All hydrogen-charged samples are in two-phases region (α-Zr and δ- hydride) at room temperature. With increasing temperature to ~420 °C, hydrogen solubility supersedes the hydrogen concentration in 331 wppm H, and a single phase hydrogen-containing α-Zr forms. Thermal diffusivity measurement shows similar temperature-dependent trends but reduced diffusivity for 331 wppm H than Zircaloy-4 at temperature above ~400 °C. This observation suggests the effect of hydrogen solution on reducing thermal diffusivity of α-Zr phase.

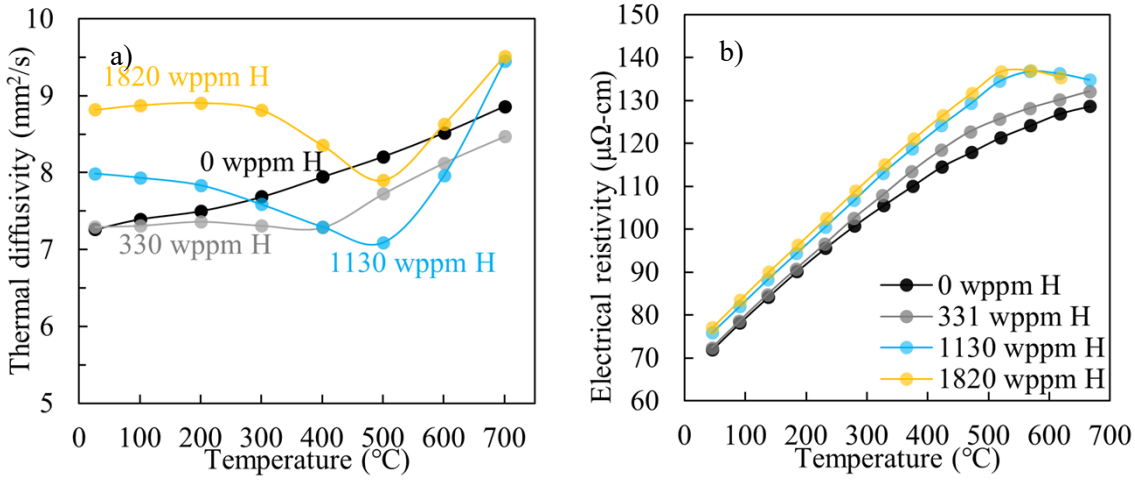

Figure 7. a) thermal diffusivity and b) electrical resistivity of hydrogen-charged Zircaloy and Zircaloy reference tube samples to three different levels.

On the other hand, a phase transformation is predicted at 550 °C, where two phases (α-Zr and β-Zr) are coexisted at higher temperature, with large hydrogen solution in β-Zr phase. This phase transformation temperature agrees with the temperature where thermal diffusivity and electrical resistivity change the trends. To support the phase transformation occurs, DSC was performed on 1130 wppm H, as the result shown in the Figure 8b. An endothermic peak occurs at 567 °C during the heating, which represent the phase transformation of α-Zr + δ-hydride to α-Zr + β-Zr phase. Note that the endothermic peaks are ~17 °C higher than thermal dynamic prediction in Figure 8. This is likely due to the non-equilibrium condition with the 20 °C/min ramping rate [34] or the effects of the alloying elements in Zircaloy-4. For example, Zircaloy-4 contained 1.2-1.7% Sn, which could act as α-Zr stabilizer, and increase the β-Zr phase transformation temperature [34, 35]. More importantly, both 1130 wppm H and 1820 wppm H exhibit similar thermal diffusivity and electrical resistivity behaviors, with the trend turnover at ~500-600 °C, which represents the phase transformation of α-Zr + δ-hydride to α-Zr + β-Zr

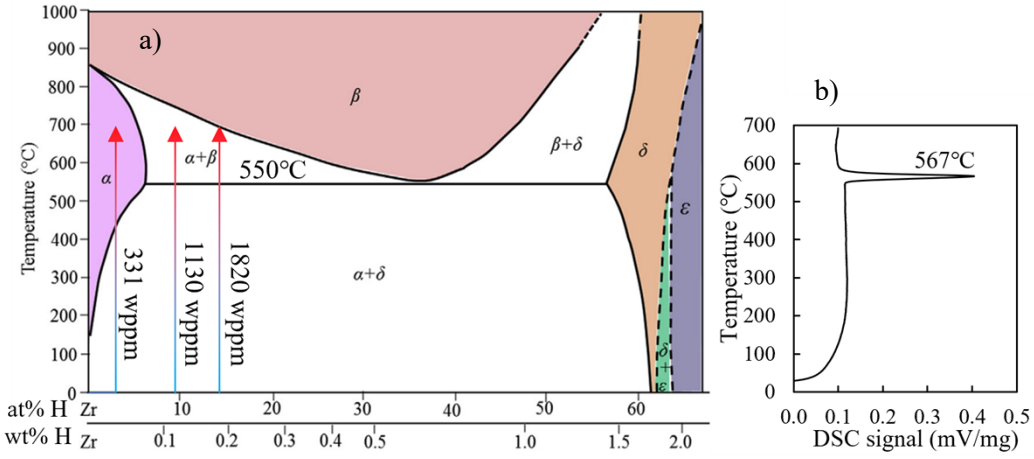

Figure 8. a) Zr H phase diagram [12, 33] with the hydrogen concentration in this work, b) DSC of 1130wppmH sample during heating at 20°C/min

3.3 Cr coatings effects

Cr coatings on Zircaloy were considered as one of the initial ATF concepts. In this work, we performed preliminary investigation of 7 μm Cr coated Zircaloy tube. This work does not serve the purpose of providing comprehensive understanding of the Cr coatings effects on the thermal diffusivity but provide preliminary results on the impact of Cr coatings on the thermal diffusivity of the cladding materials. Figure 9 shows that 7 μm Cr coatings has little impact on the thermal diffusivity of Zircaloy tubes.

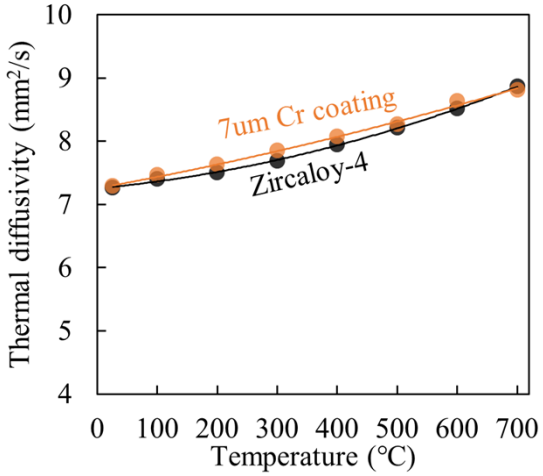

Figure 9. Thermal diffusivity of Zircaloy-4 tube, and 7um Cr coated Zircaloy tubes.

4. SUMMARY

Thermal conductivity is a critical property for Zircaloy cladding materials in nuclear reactors, as it affects the heat removal from fuels and thus has an impact on the fuel integrity. Most of the previous thermal conductivity work on Zirconium and Zircaloy was performed on plate geometry, instead of a tube geometry that is used in nuclear reactors. In this work, we used LFA to demonstrate the consistent thermal conductivity results for Zircaloy-4 tube and plate, which are in agreement with previously published data. The results prove the applicability of LFA to investigate the curve geometry specimens.

We further investigate the hydrogen effects on thermal diffusivity and electrical resistivity of Zircaloy-4 tubes. Zircaloy-4 tubes with three hydrogen concentrations (331, 1130, and 1820 wppm) were fabricated, which form δ hydride phase. The hydrogen contents play significant role in the thermal diffusivity of Zircaloy-4 tubes. The low hydrogen content Zircaloy shows relatively unchanged thermal diffusivity at temperatures below 400 ℃, but increase as a function of temperature at higher temperatures. On the other hand, the intermediate and high hydrogen content Zircaloy-4 shows a distinct temperature trend in comparison to the low hydrogen content Zircaloy-4. Both intermediate and high hydrogen content Zircaloy-4 thermal diffusivity values decrease between ~200 ℃ and 500 ℃ then start to increase at higher temperatures. A similar change of the trend occurs at similar temperatures for electrical resistivity measurements on the higher hydrogen content samples, where their electrical resistivity increases as a function of temperature below ~550℃ but then decreases at higher temperature. The change of the trends is attributed to the formation of β-Zr phase at higher temperature, supported by the thermal dynamics calculation and DSC measurement.

Cr coatings was deposited on Zircaloy-4 tube as one of the accident tolerant fuel concepts. The impact of the coatings on thermal diffusivity of Zirclaoy-4 was also investigated, with little impact from the 7 μm Cr coatings on Zircaloy

5. REFERENCES

[1] L. Xu, Y. Xiao, A. Van Sandwijk, Q. Xu and Y. Yang, "Production of nuclear grade zirconium: A review," *Journal of Nuclear Materials,* vol. 466, pp. 21-28, 2015.

[2] L. Siefken, E. W. Coryell, Harvego, E.A. and J. Hohorst, "SCDAP/RELAP5/MOD 3.3 Code Manual MATPRO - A Library of Materials Properties for Light-Water-Reactor Accident Analysis," Idaho National Engineering and Environmental Laboratory, 2001.

[3] D. Stafford, "Multidimensional simulations of hydrides during fuel rod lifecycle," *Journal of Nuclear Materials,* vol. 466, pp. 362-372, 2015.

[4] C. Tang, M. Stueber, H. J. Seifert and M. Steinbrueck, "Protective coatings on zirconium-based alloys as accident-tolerant fuel (ATF) claddings," *Corrosion Reviews,* vol. 35, pp. 141-165, 2017.

[5] K. A. Terrani, "Accident tolerant fuel cladding development: Promise, status, and challenges," *Journal of Nuclear Materials,* vol. 501, pp. 13-30, 2018.

[6] J.-C. Brachet, I. Idarraga-Trujillo, M. Le Flem, M. Le Saux, V. Vandenberghe, S. Urvoy, E. Rouesne, T. Guilbert, C. Toffolon-Masclet, M. Tupin and others, "Early studies on Cr-Coated Zircaloy-4 as enhanced accident tolerant nuclear fuel claddings for light water reactors," *Journal of Nuclear Materials,* vol. 517, pp. 268--285, 2019.

[7] T. Wei, R. Zhang, H. Yang, H. Liu, S. Qiu, Y. Wang, P. Du, K. He, X. Hu and C. Dong, "Microstructure, corrosion resistance and oxidation behavior of Cr-coatings on Zircaloy-4 prepared by vacuum arc plasma deposition," *Corrosion Science,* vol. 158, p. 108077, 2019.

[8] W. Zhong, P. A. Mouche and B. J. Heuser, "Response of Cr and Cr-Al coatings on Zircaloy-2 to high temperature steam," *Journal of Nuclear Materials,* vol. 498, pp. 137-148, 2018.

[9] D. Wongsawaeng and S. Jaiyen, "High-temperature absolute hydrogen desorption kinetics of zirconium hydride under clean and oxidized surface conditions," *Journal of Nuclear Materials,* vol. 403, pp. 19-24, 2010.

[10] A. T. Motta, L. Capolungo, L.-Q. Chen, M. N. Cinbiz, M. R. Daymond, D. A. Koss, E. Lacroix, G. Pastore, P.-C. A. Simon, M. R. Tonks, B. D. Wirth and M. A. Zikry, "Hydrogen in zirconium alloys: A review," *Journal of Nuclear Materials,* vol. 518, pp. 440--460, 2019.

[11] K. Barraclough and C. Beevers, "Some observations on the deformation characteristics of bulk polycrystalline zirconium hydrides," *Journal of Materials Science,* vol. 4, pp. 518--525, 1969.

[12] S. Suman, M. K. Khan, M. Pathak and R. Singh, "Effects of hydrogen on thermal creep behaviour of Zircaloy fuel cladding," *Journal of Nuclear Materials,* vol. 498, pp. 20-32, 2018.

[13] K. B. Colas, A. T. Motta, M. R. Daymond and J. D. Almer, "Effect of thermo-mechanical cycling on zirconium hydride reorientation studied in situ with synchrotron X-ray diffraction," *Journal of Nuclear Materials,* vol. 440, pp. 586-595, 2013.

[14] O. F. Courty, A. T. Motta, C. J. Piotrowski and J. D. Almer, "Hydride precipitation kinetics in Zircaloy-4 studied using synchrotron X-ray diffraction," *Journal of Nuclear Materials,* vol. 461, pp. 180-185, 2015.

[15] B. J. Heuser, J.-L. Lin, C. Do and L. He, "Small-angle neutron scattering measurements of δ-phase deuteride (hydride) precipitates in Zircaloy 4," *Journal of Applied Crystallography,* vol. 51, pp. 768-780, 2018.

[16] O. Zanellato, M. Preuss, J.-Y. Buffiere, F. Ribeiro, A. Steuwer, J. Desquines, J. Andrieux and B. Krebs, "Synchrotron diffraction study of dissolution and precipitation kinetics of hydrides in Zircaloy-4," *Journal of Nuclear Materials,* vol. 420, pp. 537-547, 2012.

[17] J.-l. Lin, X. Han, B. J. Heuser and J. D. Almer, "Study of the mechanical behavior of the hydride blister/rim structure in Zircaloy-4 using in-situ synchrotron X-ray diffraction," *Journal of Nuclear Materials,* vol. 471, pp. 299-307, 2016.

[18] Y. S. Kim, "Delayed hydride cracking of spent fuel rods in dry storage," *Journal of nuclear materials,* vol. 378, pp. 30-34, 2008.

[19] T. Koyanagi, H. Wang, C. M. Petrie, C. P. Deck, W.-J. Kim, D. Kim, C. Sauder, J. Braun and Y. Katoh, "Thermal diffusivity and thermal conductivity of SiC composite tubes: the effects of microstructure and irradiation," *Journal of Nuclear Materials,* vol. 557, p. 153217, 2021.

[20] J. Fink and L. Leibowitz, "Thermal conductivity of zirconium," *Journal of Nuclear Materials,* vol. 226, pp. 44-50, 1995.

[21] M. Murabayashi, S. Tanaka and Y. Takahashi, "Thermal Conductivity and Heat Capacity of Zircaloy-2,- 4 and Unalloyed Zirconium," *Journal of Nuclear Science and Technology,* vol. 12, pp. 661-662, 1975.

[22] S. Yamanaka, K. Yamada, K. Kurosaki, M. Uno, K. Takeda, H. Anada, T. Matsuda and S. Kobayashi, "Thermal properties of zirconium hydride," *Journal of Nuclear Materials,* vol. 294, pp. 94-98, 2001.

[23] S. Yamanaka, K. Yamada, K. Kurosaki, M. Uno, K. Takeda, H. Anada, T. Matsuda and S. Kobayashi, "Characteristics of zirconium hydride and deuteride," *Journal of alloys and compounds,* vol. 330, pp. 99-104, 2002.

[24] B. Tsuchiya, J. Huang, K. Konashi, M. Teshigawara and M. Yamawaki, "Thermophysical properties of zirconium hydride and uranium--zirconium hydride," *Journal of nuclear materials,* vol. 289, pp. 329-333, 2001.

[25] B. Tsuchiya, M. Teshigawara, K. Konashi and M. Yamawaki, "Thermal diffusivity and electrical resistivity of zirconium hydride," *Journal of alloys and compounds,* vol. 330, pp. 357-360, 2002.

[26] B. Maier, H. Yeom, G. Johnson, T. Dabney, J. Walters, J. Romero, H. Shah, P. Xu and K. Sridharan, "Development of cold spray coatings for accident-tolerant fuel cladding in light water reactors," *Jom,* vol. 70, pp. 198-202, 2018.

[27] T. Graening, B. Garrison, K. Kane, K. Linton and A. Nelson, "Impact of Coating Defects on Performance of Coated Zirconium Cladding," Oak Ridge National Laboratory, Oak Ridge, 2021.

[28] Y. Yan, M. Howell, B. Bevard and M. Bales, "Post-Quench Ductility Study of Zircaloy-4 Cladding under LOCA Conditions," Oak Ridge National Laboratory (ORNL/LTR-2015/106), Oak Ridge, US. , 2015.

[29] R. D. Cowan, "Pulse method of measuring thermal diffusivity at high temperatures," *Journal of Applied Physics,* vol. 34, pp. 926-927, 1963.

[30] R. Powell, R. Tye and M. Hickman, "The thermal conductivity of nickel," *International Journal of Heat and Mass Transfer,* vol. 8, pp. 679-688, 1965.

[31] T. Farrell and D. Greig, "The thermal conductivity of nickel and its alloys," *Journal of Physics C: Solid State Physics,* vol. 2, p. 1465, 1969.

[32] A. D. Feith, "Thermal conductivity and electrical resistivity of Zircaloy-4," Nuclear System Programs, Missile and Space Division, General Electrical Company, 1966.

[33] E. Zuzek, J. Abriata, A. San-Martin and F. Manchester, "The H-Zr (hydrogen-zirconium) system," *Bulletin of alloy phase diagrams,* vol. 11, pp. 385-395, 1990.

[34] R. Qiu, B. Luan, L. Chai, X. Zhang and Q. Liu, "Effects of heating rates and alloying elements (Sn, Cu and Cr) on the α→ α+ β phase transformation of Zr--Sn--Nb--Fe--(Cu, Cr) alloys," *Journal of Nuclear Materials,* vol. 453, pp. 269-274, 2014.

[35] H. Okamoto, "Sn-Zr (Tin-Zirconium)," *Journal of phase equilibria and diffusion,* vol. 31, pp. 411-412, 2010.